Chaos and relaxation to equilibrium in systems with long-range interactions

Felipe L. Antunes, Fernanda P. C. Benetti, Renato Pakter, and Yan Levin
Instituto de Física, Universidade Federal do Rio Grande do Sul, Caixa Postal 15051, CEP 91501-970, Porto Alegre, RS, Brazil
(Received 24 June 2015; revised manuscript received 17 September 2015; published 17 November 2015)

In the thermodynamic limit, systems with long-range interactions do not relax to equilibrium, but become trapped in nonequilibrium stationary states. For a finite number of particles a nonequilibrium state has a finite lifetime, so that eventually a system will relax to thermodynamic equilibrium. The time that a system remains trapped in a quasistationary state (QSS) scales with the number of particles as N^{δ}, with $\delta > 0$, and diverges in the thermodynamic limit. In this paper we will explore the role of chaotic dynamics on the time that a system remains trapped in a QSS. We discover that chaos, measured by the Lyapunov exponents, favors faster relaxation to equilibrium. Surprisingly, weak chaos favors faster relaxation than strong chaos.

DOI: 10.1103/PhysRevE.92.052123 PACS number(s): 05.20.−y, 05.45.−a, 05.70.Ln

I. INTRODUCTION

Systems in which particles interact through long-range (LR) forces remain an outstanding challenge to statistical physics. Such systems are characterized by an interparticle potential that decays with distance as $1/r^{\alpha}$, where $\alpha < d$ and d is the dimensionality of the embedding space [1–3]. Into this category fall galaxies and globular clusters [4,5], two-dimensional fluid models [6], confined plasmas [7], quantum spin models [8], dipolar systems [9], cold atoms models [10], and colloidal particles at interfaces [11]. LR interacting systems are found to have a complex relaxation process, with distinct time scales. Unlike systems in which particles interact by short-range potentials, in the thermodynamic limit LR systems do not relax to equilibrium but become trapped in out-of-equilibrium quasistationary states (QSS), the lifetime of which diverges with the number of particles. Once a system is trapped in a QSS, two outcomes are possible: if the system has a finite number of particles N, residual correlations will eventually drive it to thermodynamic equilibrium (if such equilibrium exists, which is not the case for 3D gravitational systems) after a time $t_{\times}$, which scales with N as $t_{\times} \sim N^{\delta}$, where δ is a system-specific exponent [12–14]. On the other hand, in the thermodynamic limit, $N \to \infty$, the system will remain trapped in a stationary state forever. In this collisionless limit, the relaxation to stationarity is a result of Landau damping [15–18], which transfers the energy of collective oscillations to the individual particles. Once the oscillations of the mean-field potential die out, the particles will move in a static mean-field potential. If a system has sufficient symmetry, the motion of particles in a static potential will be integrable, and the ergodicity will be irrevocably broken. This is often the case for gravitational systems whose initial particle distribution has a spherical symmetry and satisfies the generalized virial condition. On the other hand, if the initial distribution is spherically symmetric, but far from virial, strong density oscillations during the process of violent relaxation can lead to symmetry breaking [19–21]. This means that even if the initial distribution is spherically symmetric, the particle distribution and the static mean-field potential of the QSS will lack this symmetry. In general, equations of motion of a particle in a nonspherically symmetric potential are nonintegrable and chaotic orbits may be present. A natural question that arises is: will presence of chaos diminish the lifetime of a QSS, i.e., speed up the relaxation to thermodynamic equilibrium of a gravitational system [22]? That is, will a gravitational system in which spherical symmetry is spontaneously broken relax to thermodynamic equilibrium faster than a system in which this symmetry remains preserved, as suggested by Refs. [23] and [24]? Unfortunately, slow dynamics makes it very difficult to address this question in the context of self-gravitating systems. We are, therefore, forced to study simpler models that exhibit the same phenomenology as self-gravitating systems. However, even for simplified models it is very difficult to arrive at any analytical results. One possibility is to explore the Lenard-Balescu equation from plasma physics [25]. However, in order to be minimally tractable, this equation requires integrable one-particle dynamics [26], ruling out the possibility of studying the effects of chaos due to broken symmetry. In this paper we will, therefore, rely on molecular dynamics simulations to explore the effect of chaos on collisional relaxation of QSS to thermodynamic equilibrium.

II. HAMILTONIAN MEAN-FIELD MODEL

A paradigmatic model of a system with LR interactions is the Hamiltonian mean-field (HMF) model of particles moving on a circle. The Hamiltonian for this system is

$$H = \sum_{i=1}^{N} \frac{p_i^2}{2} + \frac{1}{2N} \sum_{i,j=1}^{N} [1 - \cos(\theta_i - \theta_j)], \tag{1}$$

where p_i and θ_i are the conjugate momenta and positions. If the initial particle distribution is symmetric, i.e., for each particle exists a particle in a symmetric position in phase space, the order parameter of the system—the magnetization per particle **M**—has only one nonzero vector component and can be written as

$$M = \langle \cos\theta \rangle, \tag{2}$$

where the brackets denote average over the particle distribution. The average energy per particle, $\varepsilon = H/N$, can then be expressed as

$$\varepsilon = \frac{\langle p^2 \rangle}{2} + \frac{1 - M(t)^2}{2}, \tag{3}$$

and the one-particle energy, $u_i = u(\theta_i, p_i)$, as

$$u_i = \frac{p_i^2}{2} + 1 - M(t)\cos(\theta_i), \tag{4}$$

corresponding to the energy of a single simple pendulum in a time-dependent potential. Introduced by Konishi and Kaneko as a symplectic map [27], modified to a continuous time system by Inagaki and Konishi [28], and, subsequently, presented by Antoni and Ruffo as a dynamical mean-field version of the XY spin model [29], the HMF model has been extensively studied in the literature. Depending on the overall energy of the system, the HMF has two phases: a high-energy paramagnetic (uniform) phase and a low-energy ferromagnetic (clustered) phase. The HMF model exhibits properties such as long-lived QSS, out-of-equilibrium phase transitions, and slow relaxation to thermodynamic equilibrium [1,2]. Like other LR interacting systems, the HMF model first reaches an out-of-equilibrium, nonmixed [30], QSS through a process of violent relaxation stabilized by Landau damping [31,32]. In the thermodynamic limit, $N \to \infty$, and in the ferromagnetic (clustered) phase, after the initial mean-field oscillations die out, the dynamics of spins (particles) becomes equivalent to noninteracting pendulums and chaos is absent. Integrable dynamics in the QSS prevents us from using this model to explore the role of chaos in relaxation to equilibrium. To address this question we, therefore, introduce a new model—the HMF-ladder—composed of two coupled HMFs interacting through a short-range sinusoidal potential. Since this model has two degrees of freedom, we expect that the spin dynamics of its QSS will be nonintegrable, allowing us to explore the role of chaos in relaxation to thermodynamic equilibrium.

III. HMF-LADDER MODEL

The dynamics of the conjugate momenta $\mathbf{p}_i = \{p_{\theta_i}, p_{\phi_i}\}$ and positions $\mathbf{q}_i = \{\theta_i, \phi_i\}$ of the HMF-ladder model is governed by the Hamiltonian

$$H = H_\theta + H_\phi + \epsilon \sum_{i=1}^{N} \cos(\theta_i - \phi_i), \tag{5}$$

where

$$H_\theta = \sum_{i=1}^{N} \frac{p_{\theta_i}^2}{2} + \frac{N}{2}\left(1 - M_\theta^2\right), \tag{6}$$

$$H_\phi = \sum_{i=1}^{N} \frac{p_{\phi_i}^2}{2} + \frac{N}{2}\left(1 - M_\phi^2\right), \tag{7}$$

and

$$M_\alpha = \langle \cos\alpha \rangle, \quad \alpha = \{\theta, \phi\}. \tag{8}$$

The terms given by Eqs. (6) and (7) correspond to the usual HMF model, Eq. (1). The mean energy per "particles," $\mathcal{E}$, is given by

$$\mathcal{E} = \varepsilon_\theta + \varepsilon_\phi + \epsilon \langle \cos(\theta - \phi) \rangle, \tag{9}$$

where

$$\varepsilon_\alpha = \frac{\langle p_\alpha^2 \rangle}{2} + \frac{1 - M_\alpha^2}{2}, \quad \alpha = \{\theta, \phi\}. \tag{10}$$

Unlike a simple HMF model in which particles have only one degree of freedom θ_i, positions of the "particles" of the HMF-ladder are described by a 2D vector $\mathbf{q}_i = \{\theta_i, \phi_i\}$. The dynamics of the HMF-ladder in general, therefore, will not be integrable even in a stationary state. The Hamilton equations of motion of the HMF-ladder are

$$\ddot{\theta}_i = -M_\theta \sin(\theta_i) + \epsilon \sin(\theta_i - \phi_i), \tag{11a}$$

$$\ddot{\phi}_i = -M_\phi \sin(\phi_i) - \epsilon \sin(\theta_i - \phi_i), \tag{11b}$$

where M_θ and M_ϕ are given by Eq. (8) where time is measured in units of $\tau_D = 1$. In this case, the one-particle energy, $\mathcal{U}_i = \mathcal{U}_i(\theta_i, \phi_i, p_{\theta_i}, p_{\phi_i})$, can be written as

$$\mathcal{U}_i = \frac{p_{\theta i}^2}{2} + \frac{p_{\phi_i}^2}{2} - M_\theta(t)\cos(\theta_i) - M_\phi(t)\cos(\phi_i) + \epsilon \cos(\theta_i - \phi_i) + 2, \tag{12}$$

corresponding to the energy of two coupled pendulums in a time-dependent potential.

IV. GENERALIZED VIRIAL CONDITION

In general, the dynamics of the HMF-ladder prior to its relaxation to QSS is very complicated, driven by various resonances arising from the particle-wave interactions. This makes the study of arbitrary initial conditions very difficult. There is, however, a class of initial conditions—called virial initial conditions [2]—for which the relaxation to QSS is adiabatic. Such initial distributions are particularly useful for exploring the relaxation to equilibrium, since in these cases the initial and QSS magnetizations will remain approximately the same. In this paper we will, therefore, explore the role of chaotic dynamics on the relaxation of virial initial conditions to thermodynamic equilibrium.

The virial theorem requires that in a stationary state

$$\langle p^2 \rangle = -\int d\mathbf{q}\, d\mathbf{p}\, f(\mathbf{q}, \mathbf{p}) \left[-\frac{\partial V(\mathbf{q})}{\partial \mathbf{q}} \cdot \mathbf{q} \right], \tag{13}$$

where $V(\mathbf{q})$ is the mean-field potential [2]. We expect that if the initial distribution satisfies the generalized virial condition (GVC), the macroscopic oscillations of magnetizations will be suppressed. Note that the fact that the distribution satisfies the generalized virial condition does not mean that it is already stationary. To be stationary it must be a time-independent solution of the collisionless Boltzmann (Vlasov) equation. Nevertheless, if the initial distribution satisfies the GVC, relaxation to QSS should be gentler, and strong oscillations of magnetizations should be suppressed. Furthermore, we expect that for such distributions the initial and final magnetizations will be almost the same.

The virial theorem for the HMF-ladder model is given by Eq. (13) with $\partial V(\theta, \phi)/\partial\theta = -\ddot{\theta}$, $\partial V(\theta, \phi)/\partial\phi = -\ddot{\phi}$, and $\langle p^2 \rangle = \langle p_\theta^2 \rangle + \langle p_\phi^2 \rangle$. That is,

$$\langle p_\theta^2 \rangle + \langle p_\phi^2 \rangle = -\int d\theta\, d\phi\, dp_\theta\, dp_\phi \times (\theta\ddot{\theta} + \phi\ddot{\phi}) f(\theta, \phi, p_\theta, p_\phi), \tag{14}$$

with $\ddot{\theta}$ and $\ddot{\phi}$ given by Eqs. (11). For weak coupling $\epsilon \ll |M_{\theta,\phi}|$, we use an ansatz that the virial theorem can be applied

independently to θ and ϕ subsystems, so that

$$\langle p_\theta^2 \rangle = \int d\theta\, d\phi\, dp_\theta\, dp_\phi [M_\theta \theta \sin\theta - \epsilon\theta \sin(\theta-\phi)] f(\theta,\phi,p_\theta,p_\phi), \quad (15)$$

$$\langle p_\phi^2 \rangle = \int d\theta\, d\phi\, dp_\phi\, dp_\theta [M_\phi \phi \sin\phi + \epsilon\phi \sin(\theta-\phi)] f(\theta,\phi,p_\theta,p_\phi). \quad (16)$$

Since the coupling ϵ is antiferromagnetic, the QSS magnetizations should obey $M_\theta = -M_\phi$. We, therefore, consider an initial distribution $f_0(\theta,\phi,p_\theta,p_\phi)$ composed of two antisymmetric water bags, that is,

$$f_0(\theta,\phi,p_\theta,p_\phi) = f_0^\theta(\theta,p_\theta) f_0^\phi(\phi,p_\phi), \quad (17)$$

with

$$f_0^\theta(\theta,p_\theta) = \eta_\theta \Theta(\theta_m - |\theta|)\Theta(p_m - |p_\theta|), \quad (18a)$$

$$f_0^\phi(\phi,p_\phi) = \eta_\phi \Theta(\phi_m - |\phi-\pi|)\Theta(p_m - |p_\phi|). \quad (18b)$$

The water-bag distributions in θ and ϕ are identical in momentum and have the same kinetic energy. Normalization requires that $\eta_\theta = 1/4\theta_m p_m$ and $\eta_\phi = 1/4\phi_m p_m$. The distributions are antisymmetric: f_0^ϕ is centered around π, while f_0^θ is centered on zero, with $\theta_m = \phi_m$ so $M_\theta = -M_\phi$. If the GVC is satisfied, the QSS magnetizations M_θ and M_ϕ should remain close to their initial values,

$$M_\theta = \frac{\sin\theta_m}{\theta_m}, \quad (19a)$$

$$M_\phi = -\frac{\sin\phi_m}{\phi_m}. \quad (19b)$$

Carrying out the integration in Eqs. (15) and (16) using the WB distribution Eqs. (18), we find

$$\langle p_\theta^2 \rangle = M_\theta^2 - M_\theta \cos(\theta_m) + \epsilon M_\phi \cos(\theta_m) - \epsilon M_\phi M_\theta, \quad (20a)$$

$$\langle p_\phi^2 \rangle = M_\phi^2 + M_\phi \cos(\phi_m) - \epsilon M_\theta \cos(\phi_m) - \epsilon M_\phi M_\theta, \quad (20b)$$

where we have used Eqs. (19).

The QSS magnetizations of systems whose initial distributions satisfy the GVC should be approximately the same as their initial values. We also suppose that, for a weak coupling $\epsilon \ll |M_{\theta,\phi}|$, the subsystems should remain roughly independent. Thus, we may approximate $\epsilon\langle\cos(\theta-\phi)\rangle \approx \epsilon M_\theta M_\phi$ (its initial value). Under these constraints, by conservation of energy $\langle p^2\rangle = \langle p_\theta^2\rangle + \langle p_\phi^2\rangle$ should also be preserved, and $\langle p_\theta^2\rangle = \langle p_\phi^2\rangle$ from symmetry. Therefore, we may use Eq. (9) to write

$$\langle p_{\theta,\phi}^2 \rangle = \mathcal{E} - 1 + \frac{M_\theta^2 + M_\phi^2}{2} - \epsilon M_\theta M_\phi. \quad (21)$$

Inserting the last expression in Eq. (20), and using $M_\phi = -M_\theta$, $\phi_m = \theta_m$, we obtain the GVC for the HMF-ladder, which can be written in terms of θ,

$$\mathcal{E} - 1 + M_\theta \cos\theta_m (1+\epsilon) = 0, \quad (22)$$

or of ϕ,

$$\mathcal{E} - 1 - M_\phi \cos\phi_m (1+\epsilon) = 0. \quad (23)$$

Both expressions are equivalent. Equations (22) and (23) can also be written in terms of each subsystem's mean "energy" (without the interaction term) ε_θ or ε_ϕ, given by Eq. (10). For the GVC described above, the two should be approximately equal, so we may define $\varepsilon = \varepsilon_\theta = \varepsilon_\phi$. Then, $\mathcal{E} = 2\varepsilon + \epsilon M_\theta M_\phi = 2\varepsilon - \epsilon M_\alpha^2$, $\alpha = \{\theta,\phi\}$, and the GVC reduces to

$$2\varepsilon - \epsilon M_\theta^2 - 1 + M_\theta \cos\theta_m (1+\epsilon) = 0, \quad (24a)$$

$$2\varepsilon - \epsilon M_\phi^2 - 1 - M_\phi \cos\phi_m (1+\epsilon) = 0. \quad (24b)$$

For $\epsilon = 0$, Eqs. (24) are the same as the GVC found for the HMF model [33,34].

In Fig. 1 we show the evolution of magnetizations for two initial WB distributions, calculated using molecular dynamics simulations, one of which satisfies GVC and the other one does not. As expected the oscillations of magnetization of a system that does not satisfy GVC are much more violent and the final QSS magnetization differs significantly from the initial value. On the other hand, for the WB distribution that satisfies GVC, the initial and final magnetizations are approximately the same.

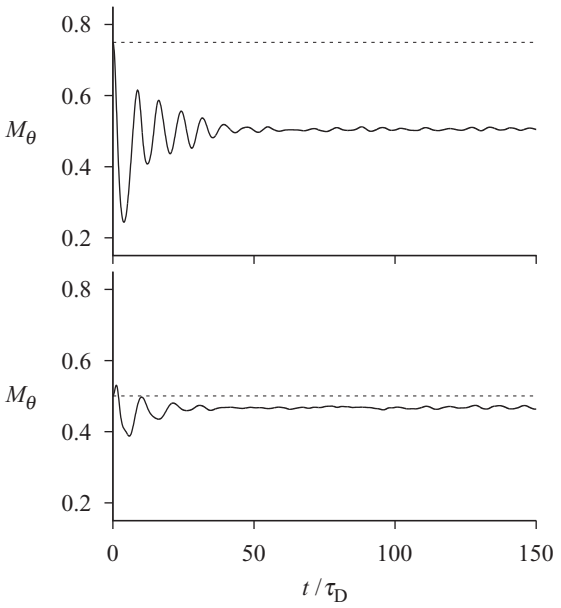

FIG. 1. Results of molecular dynamics simulations showing the short-time oscillations of the magnetization M_θ for two initial WB distributions. The top curve (solid line) is for the distribution that does not satisfy the GVC. The bottom curve (solid line) is for the initial distribution that satisfies the GVC. The horizontal dashed lines show the value of the initial magnetization for each case. Notice that for the distribution that satisfies the GVC, strong oscillations are suppressed and the final magnetization is close to the initial one. In both cases, $\epsilon = 0.1$ and $\varepsilon_\theta = \varepsilon_\phi = 0.6$, and the corresponding virial magnetization is $\sim$0.5. Due to symmetry, we show only M_θ and not M_ϕ ($M_\phi \approx -M_\theta$).

V. PARTICLE DYNAMICS

To explore the particle dynamics in a QSS we will consider Poincaré sections of test particles moving in a *fixed* mean-field potential determined by the generalized magnetizations. We are interested to study how the chaotic dynamics influences the relaxation of a QSS to thermodynamic equilibrium.

Lyapunov exponents

The central property of chaos is sensitivity to initial conditions (SIC). For a dynamical system, SIC implies that all "nearby" initial conditions result in orbits that separate exponentially fast from the original orbit. Suppose a one-dimensional dynamical system whose equation of motion is

$$\dot{x} = F(x). \tag{25}$$

Consider a given orbit, labeled a, and a second, nearby orbit, labeled b. For both orbits, we can write

$$\begin{aligned} \dot{x}_a(t) &= F(x_a), \\ \dot{x}_b(t) &= F(x_b). \end{aligned} \tag{26}$$

The distance between these orbits as a function of time is $d(t) = x_a(t) - x_b(t)$, which follows the time evolution

$$\dot{d}(t) = \dot{x}_a(t) - \dot{x}_b(t) = F(x_a) - F(x_b). \tag{27}$$

Since the second orbit begins very close to the first, we can expand $F(x_b)$ about the nearby position x_a, keeping only the first order term:

$$F(x_b) \approx F(x_a) + \left.\frac{\partial F}{\partial x}\right|_{x_a} (x_b - x_a), \tag{28}$$

$$= F(x_a) - \left.\frac{\partial F}{\partial x}\right|_{x_a} d(t). \tag{29}$$

Therefore, we can write Eq. (27) as

$$\dot{d}(t) = \left.\frac{\partial F}{\partial x}\right|_{x_a} d(t). \tag{30}$$

The largest Lyapunov exponent (LLE) λ_1 is a measure of this rate of separation: $\lambda_1 = \lim_{t\to\infty} \frac{1}{t} \ln \frac{d(t)}{d_0}$, where $d_0 = d(0)$ is the initial separation. If $\lambda_1 > 0$, the two nearby orbits will separate rapidly, and we have SIC and chaos [35,36]. Computationally, we cannot wait an infinitely long integration time, so we calculate an instantaneous Lyapunov exponent (LE) and wait long enough for this exponent to settle approximately to its asymptotic value. A strictly positive maximum Lyapunov exponent is synonymous to exponential instability [37]. A simple method of calculating the λ_1 based on its instantaneous value are provided by Benettin *et al.* [38]. In the case of the HMF-ladder, there are $4N$ Lyapunov exponents. But, for Hamiltonian flows, the Lyapunov exponent distribution (LED) has a symmetry $\lambda_i = -\lambda_{4N-i+1}$ and, since phase-space volume must be preserved, $\sum_{i=1}^{4N} \lambda_i = 0$. In addition in a QSS we have a conservation of particle energy, which, by symmetry, gives two zeros to the LED for each particle. Therefore, it is sufficient to calculate only the N largest LE, since the other exponents will be either zero or negative.

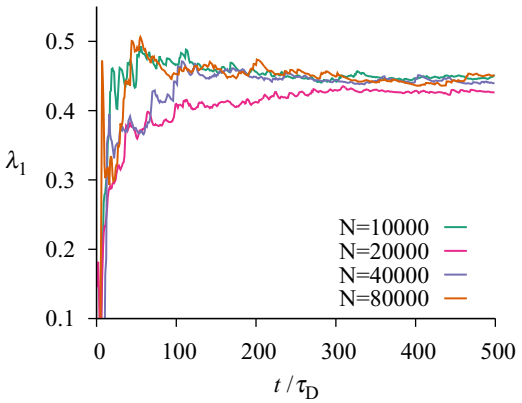

FIG. 2. (Color online) Evolution of the largest Lyapunov exponent (LLE), λ_1, to its stationary value, for the HMF model. The convergence to the same value, $\lambda_1 \simeq 0.45\,\tau_D^{-1}$, was found for different numbers of particles. This result is in agreement with the previous studies where the same behavior was observed and attributed to the instability of particles near a separatrix [40].

VI. NUMERICAL RESULTS

We have integrated the equations of motion using the fourth-order symplectic Position-Extended-Forest-Ruth-Like (PEFRL) algorithm [39] with a time step $dt = 0.1$ [38].

A. Molecular dynamics simulation

For molecular dynamics (MD) simulations of the HMF-ladder, we adopted the antisymmetric WB distribution, Eq. (18), with energy $\varepsilon_\theta = \varepsilon_\phi = 0.6$ that satisfies the GVC, Eq. (24). In Fig. 2 we first show the convergence of the LLE for the usual HMF model with the number of particles N, ranging from $N = 10^5$ to 8×10^5. We see that the final value is approximately the same for all N, $\lambda_1 \simeq 0.45\,\tau_D^{-1}$. This is a surprising result, since we expect that the particle dynamics of HMF in a QSS should be completely integrable, with LLE equal to zero. To understand better the positive value of the LLE of the HMF, we have performed a test particle dynamics simulation in which each particle moves in a *fixed, time independent,* mean-field potential determined by the initial particle distribution. We then calculated the LLE of *each* test particle. As expected, for all the particles, the LLE is zero, except for the particle near the separatrix, for which $\lambda_1 \simeq 0.28\,\tau_D^{-1}$. This result suggests that the nonvanishing LLE value found for the HMF model may be due to unstable behavior of particles near the separatrix, as was also suggested in Ref. [40]. Therefore, the LLE does not provide us with an accurate measure of the degree of chaos present in a many-body system, since its value is dominated by one unstable particle near a separatrix. Unfortunately, it is practically impossible to calculate the exact LED for $N = 10^5$ particles. We expect, however, that for initial conditions that satisfy GVC this spectrum should be similar to the spectrum of noninteracting test-particles moving in a fixed mean-field potential. The LED of test particles can be easily obtained by simply calculating the LLE of *each* test-particle of the initial distribution.

B. Test particle model simulation

To calculate the LED, we numerically integrated Eqs. (11) for the initial particle distribution of WB form satisfying

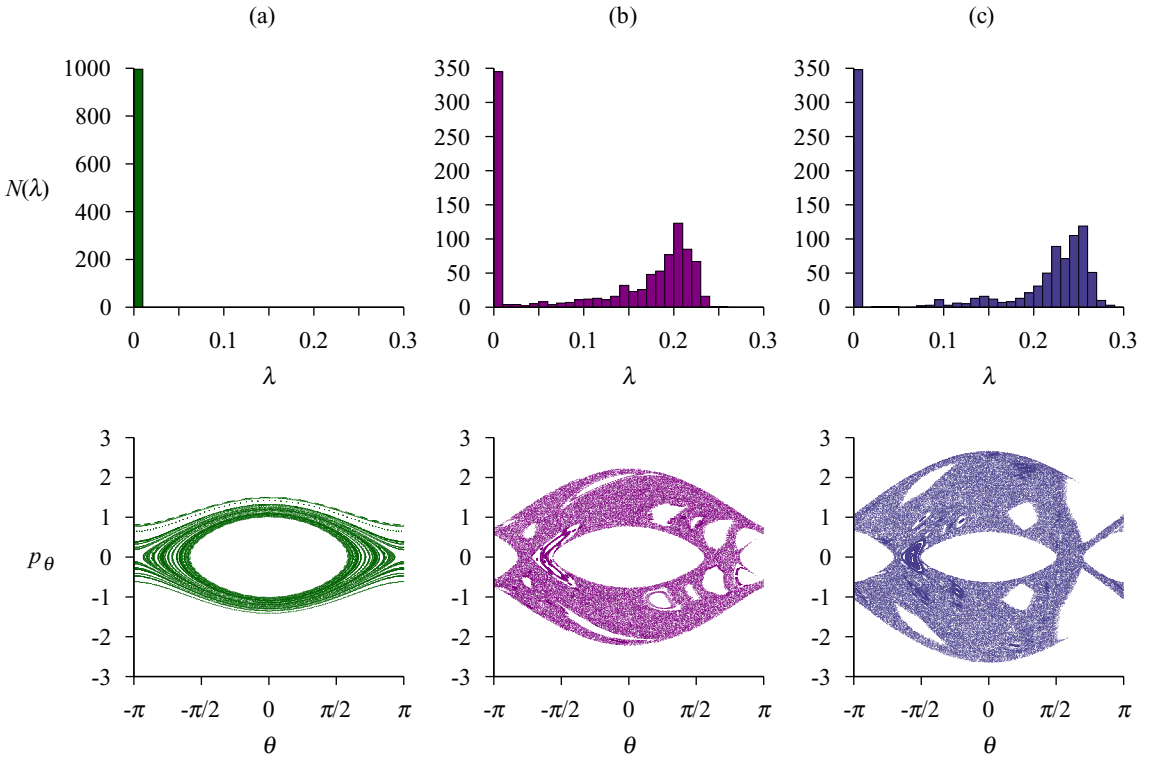

FIG. 3. (Color online) Lyapunov exponent distribution (top) and Poincaré sections (bottom) of the test-particle model for $\epsilon = 0.0$ (left column), $\epsilon = 0.5$ (middle column), and $\epsilon = 1.0$ (right column). The Poincaré sections corresponding to $\epsilon = 0.0$, $\epsilon = 0.5$, and $\epsilon = 1.0$ are of 50 test particles with energy 2.5, 2.8, and 3.2, respectively, taken when $p_\phi = 0$. We see a correlation between Poincaré sections with nonchaotic regular orbits and LED dominated by low exponents.

the GVC. The test-particles move in a time-independent mean-field potential determined by the initial magnetizations, M_θ and M_ϕ. The largest LE for each particle was obtained using the method proposed by Benettin *et al.* In the upper row of Fig. 3, we present a histogram of the LED obtained using test particle dynamics with $N = 10^5$ and different values of the coupling parameter ϵ. In the lower row, we show the characteristic Poincaré sections for the most chaotic particles near the separatrix. We see that there is a strong correlation between the LED and the Poincaré plots.

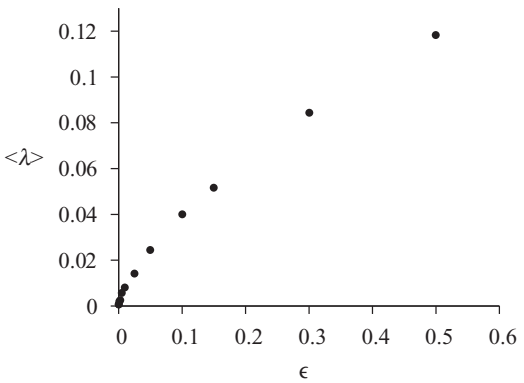

FIG. 4. Average value of the LED, $\langle\lambda\rangle$, vs. the coupling parameter ϵ. As expected, stronger coupling is related with presence of more chaos in the test-particle dynamics.

In Fig. 4 we plot the average value of the LED, as a function of the coupling parameter ϵ. For larger values of ϵ, we see that the orbits become more chaotic.

C. Relaxation exponent

To explore the relaxation to equilibrium, we study the characteristic time scale on which a system evolves from a QSS to thermodynamic equilibrium in MD simulations. As discussed previously, the crossover time scales with the number of particles as $t_\times \sim N^\delta$. We expect that the value

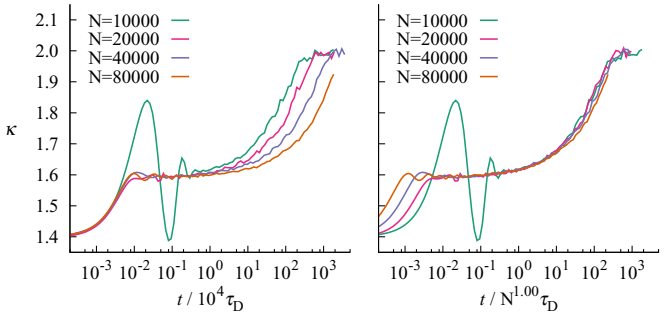

FIG. 5. (Color online) Evolution of the kurtosis for the HMF model ($\epsilon = 0.0$) with different numbers of particles, with time rescaled by $10^4\tau_D$ (left) and N^δ (right), $\delta = 1.0$. The initial particle distribution satisfied the GVC, with magnetization $M_0 = 0.431\,852$ and mean energy $\varepsilon_\theta = \varepsilon_\phi = 0.6$. The collapse suggests δ equal to 1.0, as predicted by the kinetic equation analysis developed in Ref. [41] for the HMF model.

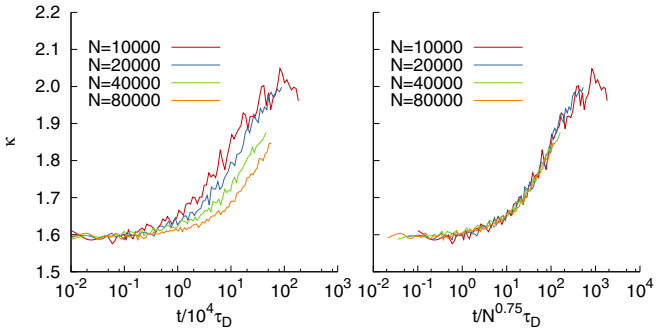

FIG. 6. (Color online) Evolution of the kurtosis for the HMF-ladder model with different numbers of particles, with time rescaled by $10^4\tau_D$ (left) and N^δ (right), $\delta = 0.75$. The initial condition satisfied the GVC, with magnetization $M_0 = 0.440\,772$, subsystem energy $\varepsilon_\theta = \varepsilon_\phi = 0.6$, and a coupling of $\epsilon = 0.01$.

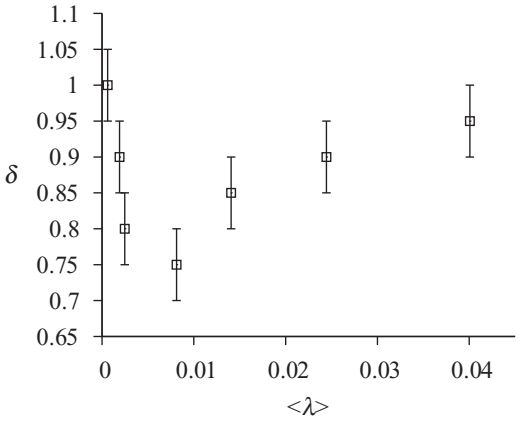

FIG. 7. Exponent δ (from the relaxation time $\tau_\times \sim N^\delta$) vs. average value of the LED, $\langle\lambda\rangle$. Each pair $(\delta, \langle\lambda\rangle)$ corresponds to a different value of the coupling parameter ϵ (see Fig. 4). We see that weak chaos favors relaxation to equilibrium more than strong chaos. Error bars restrict the range of reasonable data collapse.

of the exponent δ should be correlated with the degree of chaos present in the HMF-ladder. To calculate δ, we monitor the crossover from a QSS to thermodynamic equilibrium by measuring the momentum kurtosis given by

$$\kappa = \frac{\langle p^4 \rangle}{\langle p^2 \rangle^2}. \tag{31}$$

For the HMF-ladder in thermodynamic equilibrium, kurtosis has a universal value of two. In Figs. 5 and 6, we show the temporal evolution of kurtosis for $N = 10^3, 2 \times 10^3, 4 \times 10^3$, and 8×10^3 particles. When the time is scaled with $t_\times$ all the curves for different N and the same value of ϵ collapse onto one curve. The exponent δ is obtained by requiring the best possible data collapse; see Figs. 5 and 6. In Fig. 7 we plot the value of δ as a function of the average Lyapunov exponent. We see that the exponent δ is not a monotonic function of the amount of chaos present in a system. This is contrary to our naive expectation that the rate of relaxation to equilibrium should be proportional to the amount of chaos present in a QSS.

VII. CONCLUSIONS

We have explored the role of chaotic dynamics on the time that a system with long-range interactions remains trapped in a QSS before relaxing to thermodynamic equilibrium. The motivation for the study is provided by self-gravitating systems, which during the process of violent relaxation can suffer spontaneous symmetry breaking. When such systems relax to QSS, the resulting mean-field potential will lack spherical symmetry and the particle dynamics will be nonintegrable. The question that we wanted to address in this paper is if presence of chaotic dynamics in a nonequilibrium QSS speeds up the collisional relaxation to thermodynamic equilibrium. Unfortunately, a very slow dynamics of self-gravitating systems makes it very difficult to explore this issue. To overcome this difficulty we introduced a HMF-ladder model, which has a much simpler QSS than a self-gravitating system, characterized only by two magnetizations, M_θ and M_ϕ. With the help of this model, we have discovered that a small degree of chaos, measured by the average of LED, favors relaxation of QSS to thermodynamic equilibrium. Surprisingly, a large amount of chaos is not as efficient at driving a system to equilibrium as a small amount of chaos. Clearly chaotic dynamics of noninteracting particles cannot by itself be responsible for the relaxation to equilibrium. Nevertheless, our results suggest that there is an optimum amount of chaos that helps the residual two-body correlations drive the system toward equilibrium. At the moment we do not have any explanation for this curious behavior.

ACKNOWLEDGMENT

This work was partially supported by the CNPq, INCT-FCx, and by the US-AFOSR under Grant No. FA9550-12-1-0438.

[1] A. Campa, T. Dauxois, and S. Ruffo, Phys. Rep. **480**, 57 (2009).
[2] Y. Levin, R. Pakter, F. B. Rizzato, T. N. Teles, and F. P. C. Benetti, Phys. Rep. **535**, 1 (2014).
[3] A. Gabrielli, M. Joyce, and B. Marcos, Phys. Rev. Lett. **105**, 210602 (2010).
[4] T. Padmanabhan, Phys. Rep. **188**, 285 (1990).
[5] J. Binney and S. Tremaine, *Galactic Dynamics* (Princeton University Press, Princeton, NJ, 1987).
[6] P. H. Chavanis, J. Sommeria, and R. Robert, Astrophys. J. **471**, 385 (1996).
[7] Y. Levin, R. Pakter, and T. N. Teles, Phys. Rev. Lett. **100**, 040604 (2008).
[8] M. Kastner, Phys. Rev. Lett. **106**, 130601 (2011).
[9] O. L. Berman, R. Y. Kezerashvili, G. V. Kolmakov, and Y. E. Lozovik, Phys. Rev. B **86**, 045108 (2012).
[10] S. Slama, G. Krenz, S. Bux, C. Zimmermann, and P. W. Courteille, AIP Conf. Proc. **970**, 319 (2008).

[11] M. Oettel and S. Dietrich, Langmuir **24**, 1425 (2008).
[12] M. Joyce and T. Worrakitpoonpon, J. Stat. Mech. (2010) P10012.
[13] B. Marcos, Phys. Rev. E **88**, 032112 (2013).
[14] T. M. Rocha Filho, A. E. Santana, M. A. Amato, and A. Figueiredo, Phys. Rev. E **90**, 032133 (2014).
[15] L. Landau, J. Phys. USSR **10**, 25 (1946).
[16] D. Sagan, Am. J. Phys. **62**, 450 (1994).
[17] C.-S. Wu, Phys. Rev. **127**, 1419 (1962).
[18] C. Mouhot and C. Villani, Acta Math. **207**, 29 (2011).
[19] L. A. Aguilar and D. Merritt, Astrophys. J. **354**, 33 (1990).
[20] R. Pakter, B. Marcos, and Y. Levin, Phys. Rev. Lett. **111**, 230603 (2013).
[21] W. Simeoni, Jr., F. B. Rizzato, and R. Pakter, Phys. Plasmas **13**, 063104 (2006).
[22] Strictly speaking, for 3D gravitational systems thermodynamic equilibrium is impossible, since in infinite space particles will keep evaporating. Thermodynamic equilibrium, however, is possible for 2D gravitational systems in which particles interact by a logarithmic potential .
[23] D. Pfenniger, Astron. Astrophys. **165**, 74 (1986).
[24] H. E. Kandrup and D. E. Willmes, Astron. Astrophys. **283**, 59 (1994).
[25] P.-H. Chavanis, Astron. Astrophys. **556**, A93 (2013).
[26] P.-H. Chavanis, Eur. Phys. J. Plus **128**, 126 (2013).
[27] T. Konishi and K. Kaneko, J. Phys. A. **25**, 6283 (1992).
[28] S. Inagaki and T. Konishi, Publicat. Astron. Soc. Jpn. **45**, 733 (1993).
[29] M. Antoni and S. Ruffo, Phys. Rev. E **52**, 2361 (1995).
[30] A. Figueiredo, T. M. Rocha Filho, and M. A. Amato, Europhys. Lett. **83**, 30011 (2008).
[31] J. Barré, A. Olivetti, and Y. Y. Yamaguchi, J. Stat. Mech. (2010) P08002.
[32] J. Barré, A. Olivetti, and Y. Y. Yamaguchi, J. Phys. A **44**, 405502 (2011).
[33] F. P. C. Benetti, T. N. Teles, R. Pakter, and Y. Levin, Phys. Rev. Lett. **108**, 140601 (2012).
[34] A. C. Ribeiro-Teixeira, F. P. C. Benetti, R. Pakter, and Y. Levin, Phys. Rev. E **89**, 022130 (2014).
[35] M. Viana, *Lectures on Lyapunov Exponents* (Cambridge University Press, Cambridge, 2014).
[36] K. T. Alligood, T. D. Sauer, J. A. Yorke, and J. D. Crawford, *Chaos: An Introduction to Dynamical Systems* (Springer-Verlag, New York, 1996).
[37] With some exceptions, see the so-called Perron effect [42] .
[38] G. Benettin, L. Galgani, and J. Strelcyn, Phys. Rev. A **14**, 2338 (1976).
[39] I. P. Omelyan, I. M. Mryglod, and R. Folk, Comput. Phys. Commun. **146**, 188 (2002).
[40] F. Ginelli, K. A. Takeuchi, H. Chaté, A. Politi, and A. Torcini, Phys. Rev. E **84**, 066211 (2011).
[41] P.-H. Chavanis, J. Stat. Mech. (2010) P05019.
[42] G. A. Leonov and N. V. Kuznetsov, Int. J. Bifurcat. Chaos **17**, 1079 (2007).